Sigma Journal of Engineering and Natural Sciences
Web page info: https://sigma.yildiz.edu.tr
DOI: 10.14744/sigma.2025.000135

Research Article

Enhancing dynamic performance of turbine-generator systems with optimal SVC control using hybrid CSA-GWO technique in series-compensated networks

Sangeeta BAMBA[1,*], SK GUPTA[1]

[1]*Department of Electrical Engineering, Deenbandhu Chhotu Ram University of Science and Technology, Sonipat, Haryana, 131001, India*

ARTICLE INFO

Article history
Received: 22 November 2024
Revised: 15 January 2025
Accepted: 19 February 2025

Keywords:
Hybrid Cuckoo Search Algorithm-Gray Wolf Optimization (CSA-GWO) Technique; Static Var Compensator (SVC); Sub Synchronous Resonance (SSR)

ABSTRACT

This paper presents a comprehensive study on enhancing the dynamic performance of a turbine-generator set connected to an infinite busbar, with a primary focus on mitigating sub-synchronous resonance in a series-compensated transmission network. SSR is a critical phenomenon that threatens turbine-generator systems by inducing harmful oscillations in generator rotor shafts, potentially leading to severe damage. To address this issue, the study employs the IEEE first benchmark model, without natural damping, and proposes a robust solution involving a Static Var Compensator coupled with an optimal controller optimized through a hybrid Cuckoo Search Algorithm-Gray Wolf Optimization approach, benchmarked against the Bacterial Foraging Optimization Algorithm. The study considers zero inherent damping to simulate the most severe conditions, while natural damping is included for comparative analysis. Eigenvalue analysis and MATLAB Power System Blockset simulations demonstrate significant improvements in system damping characteristics, with eigenvalues shifting towards the left half-plane and a notable reduction in peak rotor shaft oscillations compared to BFOA-based control. Time-domain analysis confirms the system›s effectiveness, with the hybrid CSA-GWO technique achieving superior damping, minimal peak time variation, and the best improvement in settling time and overshoot, especially at higher series compensation levels. The study concludes that the hybrid CSA-GWO-based controller not only enhances the system›s response to disturbances but also outperforms over BFOA Algorithm, offering faster, more effective mitigation of SSR and significantly improving the dynamic performance of the turbine-generator system.

Cite this article as: Bamba S, Gupta SK. Enhancing dynamic performance of turbine-generator systems with optimal SVC control using hybrid CSA-GWO technique in series-compensated networks. Sigma J Eng Nat Sci 2026;44(2):1419–1439.

***Corresponding author.**
*E-mail address: 20001902005sangeetabamba@dcrustm.org

This paper was recommended for publication in revised form by Editor-in-Chief Ahmet Selim Dalkilic

INTRODUCTION

The rapid expansion of power systems and the integration of renewable energy sources have introduced new complexities into grid dynamics, particularly in mitigating adverse effects such as sub-synchronous resonance (SSR). SSR is an electrical resonance condition that occurs when the natural frequency of mechanical oscillations in turbine-generators coincides with sub-synchronous frequencies in the electrical network. This phenomenon can lead to significant system instability and potentially catastrophic damage to turbine-generator shafts. Therefore, effective SSR mitigation strategies have become crucial in maintaining power system stability and preventing mechanical failures.

SSR was first identified in the 1970s with the integration of series capacitors in transmission lines, a practice aimed at enhancing power transfer capability [1]. When mechanical and electrical resonant frequencies align, turbine-generator shafts experience sustained oscillations, resulting in severe mechanical stresses[2]. Notable incidents like the Navajo and Mohave projects[3] highlighted the destructive potential of SSR in real-world applications [4]. Over time, various mitigation strategies have been proposed, with substantial advancements in technology and research contributing to improved system stability.

One of the most notable innovations in SSR mitigation is the introduction of Flexible AC Transmission Systems (FACTS). FACTS devices such as Static VAR Compensators (SVC) and Static Synchronous Compensators (STATCOM) offer advanced solutions to enhance grid stability and damp power oscillations, including SSR. Padiyar [5] emphasized the role of FACTS controllers in addressing grid stability issues. However, the increasing complexity of modern grids, especially with the growing penetration of renewable energy sources, has created a demand for more sophisticated approaches that combine traditional methods with optimization algorithms and advanced control techniques.

The advent of FACTS technology revolutionized SSR mitigation by offering dynamic solutions for power system stability. FACTS devices like SVCs were initially explored by Narendra Kumar and Dave [6]for damping SSR, demonstrating their effectiveness in enhancing system stability. Similarly, Padiyar and Prabhu[7] investigated the use of STATCOM for SSR damping, further demonstrating the potential of FACTS devices in managing grid dynamics.

As renewable energy sources become increasingly integrated into power grids, new challenges have emerged in SSR mitigation. Recent studies have explored the interaction between renewable energy systems and SSR. For instance, Prada et al. [8] examined the role of Type-2 wind turbines in damping SSR, study [9,10] proposed intelligent STATCOM control strategies to enhance stability during torsional oscillations in systems with high renewable penetration.

Despite their effectiveness, traditional FACTS controllers rely on fixed control parameters, which limits their adaptability to dynamic grid conditions. As power systems evolve, the increasing penetration of renewable energy sources[11] introduces unpredictable variations, requiring advanced control strategies that enhance the responsiveness and efficiency of SSR mitigation[12]

To overcome the limitations of conventional SSR mitigation strategies, researchers have increasingly turned to soft computing and optimization techniques. Metaheuristic algorithms, such as Cuckoo Search Optimization (CSO) [8], Grey Wolf Optimizer (GWO) [13], and Quantum-behaved Particle Swarm Optimization (QPSO) [14], have been successfully applied to enhance FACTS-based damping controllers. These algorithms offer improved controller tuning, real-time adaptation, and enhanced SSR suppression [15].

Additionally, hybrid optimization approaches combining multiple algorithms—such as Cuckoo Search Algorithm with Grey Wolf Optimizer (CSA-GWO)—have demonstrated superior performance in mitigating SSR. These techniques leverage the strengths of individual algorithms, optimizing STATCOM and SVC controllers to effectively damp sub-synchronous oscillations. Recent studies, including Bamba and Gupta [11], have explored intelligent STATCOM control strategies for enhancing system stability, particularly in grids with high renewable penetration.

Several challenges complicate SSR analysis and mitigation in modern power systems. First, the increased complexity of grid dynamics, driven by renewable energy integration and enhanced interconnectivity, makes it difficult to predict SSR behavior accurately. Second, real-time optimization of SSR mitigation strategies requires significant computational power and efficient algorithms capable of adapting to changing grid conditions. Finally, ensuring the interoperability of FACTS devices and SSR damping controllers [16] with various grid components, including renewable energy sources, is essential to maintaining overall system stability.

This study aims to bridge the research gap by proposing an advanced FACTS-based SSR mitigation strategy, leveraging hybrid optimization techniques to improve controller adaptability, dynamic stability, and overall power system resilience.

This paper aims to address these challenges by proposing advanced SSR mitigation strategies that combine FACTS technology with optimization algorithms and machine learning techniques, offering a comprehensive solution for modern power grids. Following reference, Table 1 provides a comparative analysis between the proposed work and the existing cutting-edge research.

Table 1. Comparison of SSR mitigation strategies and control approaches

Reference	System Type	Compensation Method	Controller Gain Selection	Key Points
[2][**1990**]	Series-Compensated Systems	SSR damping with series compensation	Not specified	Foundational study on SSR and its impact on turbine-generator interactions.
[3,17], [**1997**]	Navajo Project	SSR analysis and mitigation	Not specified	Detailed mitigation strategies from the Navajo project.
[17],[**2002**]	General Power Systems	SVC-based damping	Optimized using auxiliary control	Explored SSR damping through SVC and auxiliary control mechanisms.
[7], [**2006**]	Series-Compensated Systems	STATCOM for SSR damping	Optimized for system stability	Demonstrated the effectiveness of STATCOM in mitigating SSR.
[10],[**2023**]	Multi-source Systems	Cuckoo Search Optimization for AGC	Optimized using Cuckoo Search	Applied modern optimization techniques for improved SSR damping.
[13], [**2023**]	Series-Compensated Power Systems	GWO-based control for SSR mitigation	Optimized using Grey Wolf Optimizer	Applied modern optimization techniques for improved SSR damping.
[9], [**2024**]	Series-Compensated Power Systems		STATCOM-based PI Controller.	Damp torsional oscillations.

Novelty and its Main Contribution

This paper aims to contribute to the field by:

- The paper proposes the use of a Static Var Compensator (SVC) as an effective device to damp electromechanical oscillations in turbine-generator systems. SVC improves the system›s voltage stability and enhances its overall response to dynamic disturbances.
- In addition to this, study presents an optimal control design for SVC using the CSA-GWO technique, which uses all the system states as feedback to stabilize the output to handle higher levels of series compensation. The hybrid optimization approach leads to a controller design that minimizes SSR risks while enhancing the dynamic performance of the turbine-generator system.
- The study introduces a hybrid optimization approach that combines the strengths of Cuckoo Search Algorithm (CSA) and Gray Wolf Optimization (GWO) to optimize the control parameters of optimal SVC in mitigating SSR.
- The proposed CSA-GWO-based controller is benchmarked against the Bacterial Foraging Optimization Algorithm (BFOA), demonstrating superior performance in terms of convergence speed and system stability.
- The effectiveness of the proposed solution is validated through eigenvalue analysis and MATLAB simulations, providing a detailed comparison of system performance under different levels of damping i.e with and without natural damping.

The manuscript is organized as follows: Section 2 presents the system overview, including the IEEE First Benchmark Model. Section 3 outlines the mathematical model, while Section 4 explores optimal control theory. Section 5 introduces the Hybrid CSA-GWO technique for enhanced system performance. Finally, the Results and Discussion Section 6 provides an in-depth analysis of the findings.

SYSTEM OVERVIEW

The system under consideration consists of several key components. First, it includes a turbine-generator system that is represented by the IEEE first benchmark model, which is commonly used for studying Sub-Synchronous Resonance (SSR) and its effects. Additionally, the system features a series-compensated transmission network, which enhances power transfer capability but also introduces the risk of SSR by potentially exciting sub synchronous oscillations. To address these challenges, a Static Var Compensator (SVC) is employed for reactive power compensation and voltage control, helping to stabilize the system under varying operating conditions. Furthermore, an optimal controller is designed using a hybrid CSA-GWO (Cuckoo Search Algorithm - Gray Wolf Optimization) technique, which enhances overall system stability by effectively damping SSR and improving dynamic performance.

IEEE First Benchmark Model

The IEEE first benchmark model, widely used for SSR studies, comprises several key components as shown in Figure 1. It includes a three-phase, salient-pole synchronous generator, and a mechanical system that features the generator rotor, low-pressure turbine, high-pressure turbine, and

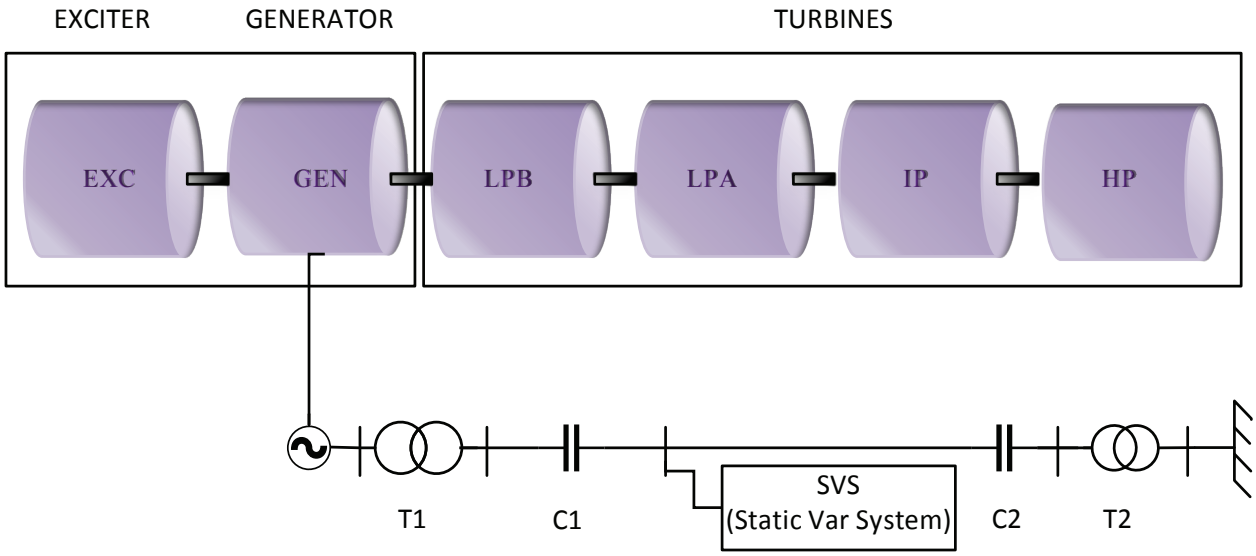

Figure 1. Modified IEEE first benchmark model with svc.

exciter, all modeled as multi-mass shafts. Additionally, the model incorporates an excitation system that regulates terminal voltage and reactive power using a voltage reference signal. Furthermore, it features a series-compensated network that introduces capacitive compensation to enhance power transfer, which can excite SSR modes.

MATHEMATICAL MODELING

Generator

A generalized system model for a synchronous machine, as depicted in Figure 2, was considered. To address the challenges associated with dynamic saliency, the concept of dummy coils is utilized, as discussed by [5]. The generator model comprises a 'field winding, f' with a 'damper winding, h' along the d-axis, and 'two damper windings, g and k' along the q-axis[18].

The rotor flux linkages, denoted as 'Ψ', associated with various windings, lead to the following rotor equations:

$$\frac{d\psi_f}{dt} = a_1.\psi_f + a_2\psi_h + b_1 v_f + b_2 i_d \tag{1}$$

$$\frac{d\psi_f}{dt} = a_3.\psi_f + a_4\psi_h + b_3 i_d \tag{2}$$

$$\frac{d\psi_f}{dt} = a_5.\psi_g + a_6\psi_k + b_4 v_g + b_5 i_q \tag{3}$$

$$\frac{d\psi_f}{dt} = a_7.\psi_g + a_8\psi_k + b_6 i_q \tag{4}$$

Here, (V_f) represents the field excitation voltage. These equations are linearized and transformed into the D-Q frame of reference, as described by Ramsaw and Padiyar (1973). The resulting state space model is as follows:

$$\begin{aligned}
&\dot{X}_R = [A_R]X_R + [B_{R1}]U_{R1} + B_{R2}[U_{R2}] + [B_{R3}]U_{R3} \\
&X_R = \begin{bmatrix}\Delta\psi_f & \Delta\psi_f & \Delta\psi_f & \Delta\psi_k\end{bmatrix}^t \\
&U_{R1} = \begin{bmatrix}\Delta\delta & \Delta\omega\end{bmatrix}^t \\
&U_{R2} = \begin{bmatrix}\Delta V_F\end{bmatrix} \\
&U_{R3} = \begin{bmatrix}\Delta i_D & \Delta i_Q\end{bmatrix}^t \\
&Y_{R1} = [C_{R1}]X_R + [D_{R1}]U_{R1} \\
&Y_{R2} = [C_{R2}]X_R + [D_{R2}]U_{R2} + [D_{R3}]U_{R3} + [D_{R3}]U_{R3} \\
&Y_{R1} = \begin{bmatrix}\Delta I_D \\ \Delta I_Q\end{bmatrix}, Y_{R1} = \begin{bmatrix}\Delta I_D \\ \Delta I_Q\end{bmatrix}
\end{aligned} \tag{5}$$

Mechanical System

The mechanical system, illustrated in Figure 3, is represented by the spring-mass model. The fundamental equations governing this system, along with the state and output equations, are detailed as follows:

$$\frac{d\omega_1}{dt} = \left[\frac{-(D_{11}+D_{12})(\omega_1-\omega_0) + D_{12}(\omega_2-\omega_0) - K_{12}(\delta_1-\delta_2) + T_{M1}}{M_1}\right] \tag{6}$$

$$\frac{d\omega_2}{dt} = \left[\frac{D_{12}(\omega_1-\omega_0) - (D_{12}+D_{22}+D_{23})(\omega_2-\omega_0) + D_{23}(\omega_3-\omega_0) - K_{12}(\delta_2-\delta_1) - K_{23}(\delta_2-\delta_3) + T_{M2}}{M_2}\right] \tag{7}$$

$$\frac{d\omega_3}{dt} = \left[\frac{D_{23}(\omega_2-\omega_0) - (D_{23}+D_{33}+D_{34})(\omega_3-\omega_0) + D_{34}(\omega_4-\omega_0) - K_{23}(\delta_3-\delta_2) - K_{34}(\delta_3-\delta_4) + T_{M3}}{M_3}\right] \tag{8}$$

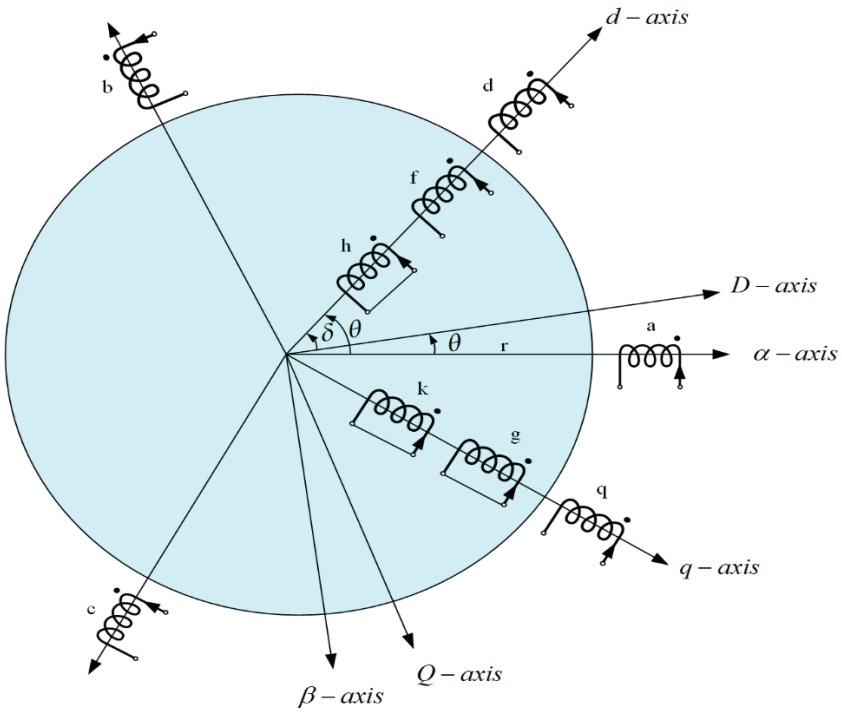

Figure 2. Generator model with four damping winding.

$$\frac{d\omega_4}{dt}=\left[\frac{D_{34}(\omega_3-\omega_0)-(D_{34}+D_{44}+D_{45})(\omega_2-\omega_0)+D_{45}(\omega_5-\omega_0)-K_{34}(\delta_4-\delta_3)-K_{45}(\delta_4-\delta_5)+T_{M4}}{M_4}\right] \quad (9)$$

$$\frac{d\omega_5}{dt}=\left[\frac{D_{45}(\omega_4-\omega_5)-(D_{56}+D_{45}+D_{55})(\omega_5-\omega_0)+D_{56}(\omega_6-\omega_0)-K_{45}(\delta_5-\delta_4)-K_{56}(\delta_5-\delta_6)+T_E}{M_5}\right] \quad (10)$$

$$\frac{d\omega_6}{dt}=\left[\frac{-(D_{56}+D_{66})(\omega_6-\omega_0)+D_{56}(\omega_5-\omega_0)-K_{56}(\delta_6-\delta_5)}{M_6}\right] \quad (11)$$

$$\omega_i=\frac{d\delta_i}{dt}\text{ , Where i= 1 to 6}$$

$$T_E=-X_D{}''\left(i_D I_Q-i_Q I_D\right) \quad (12)$$

In Figure 3, the variables (i) and (i) represent the angular position and velocity of the i[th] mass of various shaft segments, respectively, where (i) ranges from 1 to 6.

By linearizing these equations, we derive the state space model as follows:

$$\Delta T_{M1}=\Delta T_{M2}=\Delta T_{M3}=\Delta T_{M4}=0$$

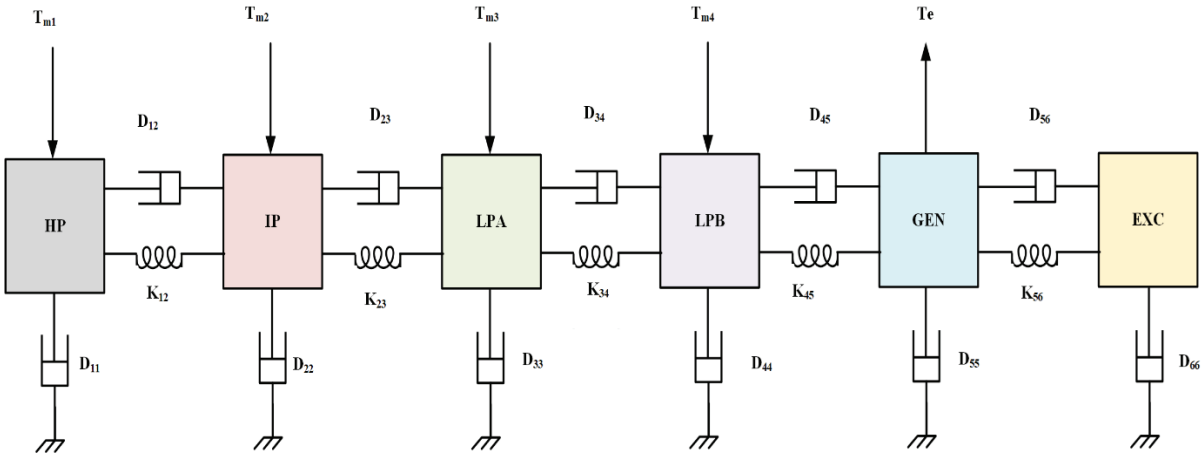

Figure 3. Six spring mass model of mechanical system.

Given that the governor system operates with significant time constants

$$\dot{X}_m = [A_M]X_M + [B_{M1}]U_{M1} + [B_{M2}]U_{M2} \quad (13)$$

$$Y_M = [C_M]X_M \quad (14)$$

Where, $X_M = [\Delta\delta_1 \quad \Delta\delta_2 \quad \Delta\delta_3 \quad \Delta\delta_4 \quad \Delta\delta_5 \quad \Delta\delta_6 \quad \Delta\omega_1 \quad \Delta\omega_2 \quad \Delta\omega_3 \quad \Delta\omega_4 \quad \Delta\omega_5 \quad \Delta\omega_6]$

$$Y_M = [\Delta\delta_5 \quad \Delta\omega_5]^t$$

$$U_{M1} = [\Delta I_D \quad \Delta I_Q]^t$$

$$U_{M2} = [\Delta i_D \quad \Delta i_Q]^t$$

Excitation System

The IEEE type-1 model, depicted in Figure 4, illustrates the excitation system. In this model, (Vg) denotes the generator terminal voltage, while (S_E) represents the saturation function. The excitation system is characterized by the following set of equations:

$$\frac{dv_F}{dt} = \left[\frac{-(K_E + S_E)}{T_E}\right]v_F + \frac{v_R}{T_E} \quad (15)$$

$$\frac{dv_s}{dt} = -\left[\frac{K_F(K_E + S_E)}{(T_E T_F)}\right]v_F + \frac{v_s}{T_E} + \frac{K_F v_R}{T_E T_F} \quad (16)$$

$$\frac{dv_R}{dt} = \frac{K_A V_{ref}}{T_A} - \frac{K_A v_s}{T_A} - \frac{K_A v_G}{T_A} - \frac{v_R}{T_A} \quad (17)$$

$$S_E = A_E . e^{(B_E V_F)} \quad (18)$$

$$\dot{X}_E = [A_E]X_E + [B_E]U_E \quad (19)$$

$$Y_E = [C_E]X_E \quad (20)$$

The resulting linearized state and output equations are as follows:

$$X_E = [\Delta v_F \quad \Delta v_S \quad \Delta v_R]^t \quad (21)$$

$$Y_E = [\Delta v_F] \quad (22)$$

$$U_E = [\Delta V_g]^t \quad (23)$$

Network

The transmission line modeled using lumped parameters in a π-circuit configuration. The network is depicted by its α-axis equivalent circuit, which is identical to the positive sequence network. The governing equations for the α-axis and π-network representation are derived as follows:

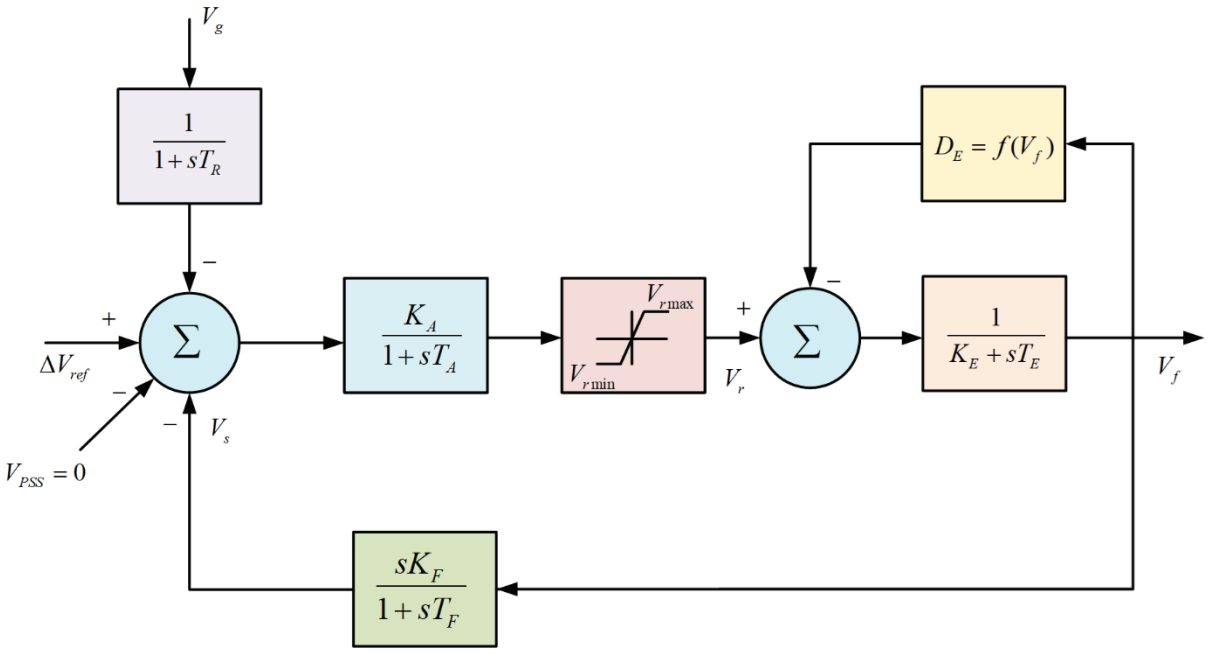

Figure 4. IEEE type-1 excitation system.

$$\frac{di_{1a}}{dt} = \frac{v_{2\alpha}}{L_{T2}} - \frac{v_{1\alpha}}{L_{T2}} - \frac{v_{3\alpha}}{L_{T2}} \quad (24)$$

$$\frac{di_{2a}}{dt} = -i_{2\alpha}\left[\frac{R_r}{L_r}\right] - \frac{v_{2\alpha}}{L_r} - \frac{v_{3\alpha}}{L_r} \quad (25)$$

$$\frac{di_{4a}}{dt} = -i_{4\alpha}\left[\frac{R_s}{L_s}\right] - \frac{v_{3\alpha}}{L_s} - \frac{v_{4\alpha}}{L_s} \quad (26)$$

$$\frac{di_a}{dt} = -\frac{R_a i_\alpha}{L_A} - \frac{v_{4\alpha}}{L_A} - \left(\frac{L''_d}{L_A}\right)\left[\frac{dI_\alpha}{dt}\right] - \frac{v_{6\alpha}}{L_A} \quad (27)$$

$$\frac{dv_{2\alpha}}{dt} = -\left(\frac{1}{C_r}\right)i_{2\alpha} - \left(\frac{1}{C_r}\right)i_{1\alpha} \quad (28)$$

$$\frac{dv_{3\alpha}}{dt} = -\frac{i_{2\alpha}}{C_n} - \frac{i_{3\alpha}}{C_n} + \frac{i_{4\alpha}}{C_n} \quad (29)$$

$$\frac{dv_{4\alpha}}{dt} = -\frac{i_\alpha}{C} - \frac{i_{4\alpha}}{C_n} \quad (30)$$

$$\frac{dv_{5\alpha}}{dt} = -\frac{i_{1\alpha}}{C_{se2}} \quad (31)$$

$$\frac{dv_{6\alpha}}{dt} = -\frac{i_\alpha}{C_{se1}} \quad (32)$$

$$v_{ga} = R_\alpha i_\alpha + L''_D\left(I'_\alpha + I'_\alpha\right) \quad (33)$$

$$v_{ga} = R_\alpha i_\beta + L''_D\left(I'_\beta + I'_\beta\right) \quad (34)$$

$$L_A = L_{T1} + L''_D \quad (35)$$

$$L_s = L_r = \frac{L}{2} \quad (36)$$

$$C_s = C_r = \frac{C}{2} \quad (37)$$

$$R_s = R_r = \frac{R}{2} \quad (38)$$

The line inductance and resistance are denoted by (L) and (R), respectively. In a similar manner, equations can be formulated for the β-network. These α-β network equations are then transformed into the DQ frame of reference. By linearizing these differential equations around the operating point, we obtain the state space model equations for the transmission network system.

$$\dot{X}_N = [A_N]X_N + [B_{N1}]U_{N1} + [B_{N2}]U_{N2} + [B_{N3}]U_{N3} \quad (39)$$

$$Y_{N1} = [C_{N1}]X_N + [D_{N1}]U_{N1} + [D_{N2}]U_{N2} + [D_{N3}]U_{N3} \quad (40)$$

$$Y_{N2} = [C_{N2}]X_N \quad (41)$$

$$Y_{N3} = [C_{N3}]X_N \quad (42)$$

Where,

ΔV_{4D} ΔV_{5D} ΔV_{6D} Δi_{1Q} Δi_{2Q} Δi_{4Q} Δi_Q ΔV_{2Q} ΔV_{3Q} ΔV_{4Q} ΔV_{5Q}]

$$U_{N1} = \begin{bmatrix}\Delta i_{3D}\\ \Delta i_{3Q}\end{bmatrix}, U_{N2} = \begin{bmatrix}\Delta I_D\\ \Delta I_Q\end{bmatrix}, U_{N3} = \begin{bmatrix}\dot{\Delta} I_D\\ \dot{\Delta} I_Q\end{bmatrix},$$

$$Y_{N1} = \begin{bmatrix}\Delta V_{gD}\\ \Delta V_{gQ}\end{bmatrix}, Y_{N2} = \begin{bmatrix}\Delta i_D\\ \Delta i_Q\end{bmatrix}, Y_{N3} = \begin{bmatrix}\Delta V_{3D}\\ \Delta V_{3Q}\end{bmatrix}$$

The matrices AN, BN1, BN2, BN3, CN1, DN1, DN2, DN3, CN2, and CN3 are derived from the works of Anderson et al. (1990) and Padiyar (2009)

Static Var Compensator

The Static Var Compensator (SVC) is a shunt device used for reactive power compensation and voltage regulation in power systems. It comprises a Thyristor-Controlled Reactor (TCR) and a fixed capacitor, regulated by a Proportional-Integral (PI) controller for stable voltage control. The linearized SVC control model includes TCR transients and delays from the controller and measurement units, accounting for thyristor switching behavior and signal processing times as shown in Figure 5. TCR currents are expressed in α-axis and β -axis components, simplifying the three-phase system dynamics. These features are key for maintaining voltage stability in dynamic power environments

The currents entering the TCR from the network along the α and β axes are expressed as follows:

$$L_s\frac{di_{3\alpha}}{dt} + R_s i_{3\alpha} = V_{3\alpha} \quad (43)$$

$$L_s\frac{di_{3\beta}}{dt} + R_s i_{3\beta} = V_{3\beta} \quad (44)$$

By applying Kron's transformation to the equations, which involves converting them into the D-Q frame of reference and subsequently linearizing them around the operating point, we obtain the following results:

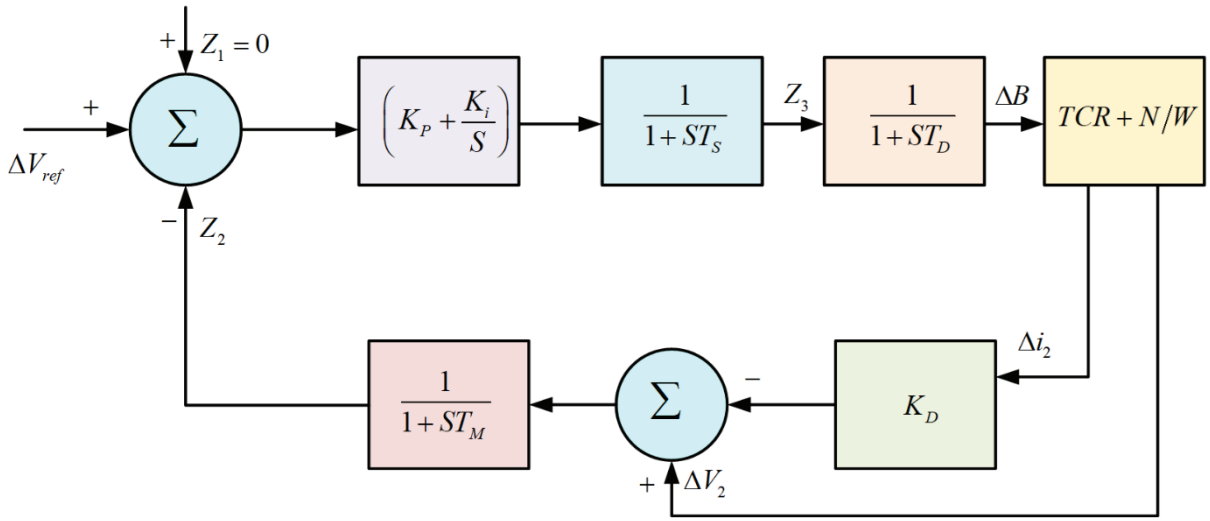

Figure 5. SVS control model.

$$\begin{bmatrix}\Delta i_{3D}\\ \Delta i_{3Q}\end{bmatrix} = \begin{bmatrix}-R_s/L_s & -w_0\\ -w_0 & -R_s/L_s\end{bmatrix}\begin{bmatrix}\Delta i_{3D}\\ \Delta i_{3Q}\end{bmatrix} + \begin{bmatrix}w_0B_0 & 0\\ 0 & w_0B_0\end{bmatrix}\begin{bmatrix}\Delta v_{3D}\\ \Delta v_{3Q}\end{bmatrix} + w_0\begin{bmatrix}\Delta v_{3D0}\\ \Delta v_{3Q0}\end{bmatrix}\Delta B \quad (45)$$

Here, $Q = \frac{\omega_0 L_S}{R_S}$ and

$B = \frac{1}{\omega_0 L_S}$

In this context, (Ls) and (Rs) denote the inductance and resistance of the TCR, respectively. The linearized state and output equations for the SVS model are formulated as follows:

$$\dot{X}_S = [A_S]X_S + [B_{S1}]U_{S1} + [B_{S2}]U_{S2} + [B_{S3}]U_{S3} \quad (46)$$

The additional equations derived from the SVS control model are as follows:

$$\frac{d\Delta B}{dt} = \frac{Z_3}{T_D} - \frac{\Delta B_3}{T_D} \quad (47)$$

$$\frac{dZ_2}{dt} = 1/T_M\left[\Delta V_3 - Z_2 + K_D\Delta i_3\right] \quad (48)$$

$$\frac{dZ_3}{dt} = -1/T_S\left[Z_3 - K_1Z_1 + K_P\Delta V_{ref} - K_PZ_2 + K_P\Delta v_F\right] \quad (49)$$

where ΔV_{ref} represents the 'reference voltage perturbation', ΔV_f is the output of the 'auxiliary controller', and ΔV_3 and Δi_3 denote the 'incremental magnitudes of the SVS bus voltage and TCR current', respectively. The 'SVS bus voltage' V_3 is expressed in terms of its DQ-axis components as follows:

$$V_2^2 = V_{2D}^2 + V_{2Q}^2 \quad (50)$$

The magnitude of the TCR currents is expressed as follows:

$$i_2^2 = i_{2D}^2 + i_{2Q}^2 \quad (51)$$

The output equations derived are as follows:

$$Y_S = [C_S]X_S + [D_S]U_{S1} \quad (52)$$

$$X_S = \left[\Delta i_{3D} \quad \Delta i_{3Q} \quad Z_1 \quad Z_2 \quad Z_3 \quad \Delta B\right]^t$$

$$Y_S = \left[\Delta i_{3Q} \quad \Delta i_{3Q}\right]^t$$

$$U_{S2} = \left[\Delta V_{ref}\right]$$

$$U_{S3} = \left[\Delta V_f\right]$$

The matrices AS, BS1, BS2, BS3, CS, and DS are derived from the works of Anderson et al. (1990) and Padiyar (2009). The overall system model is shown in Figure 6.

Optimal Control Theory

The comprehensive system model, which integrates the generator model, mechanical model, excitation system, network model, and SVS model, can be represented using "optimal control theory".

$$\dot{X} = AX(t) + Bu(t) + Fw \quad (53)$$

Above equation is utilized in optimal control theory (Kothari and Nagrath, 2007), and its Performance Index (PI) is given below:

$$PI = \frac{1}{2}\int_0^\infty (X'QX' + RU') \quad (54)$$

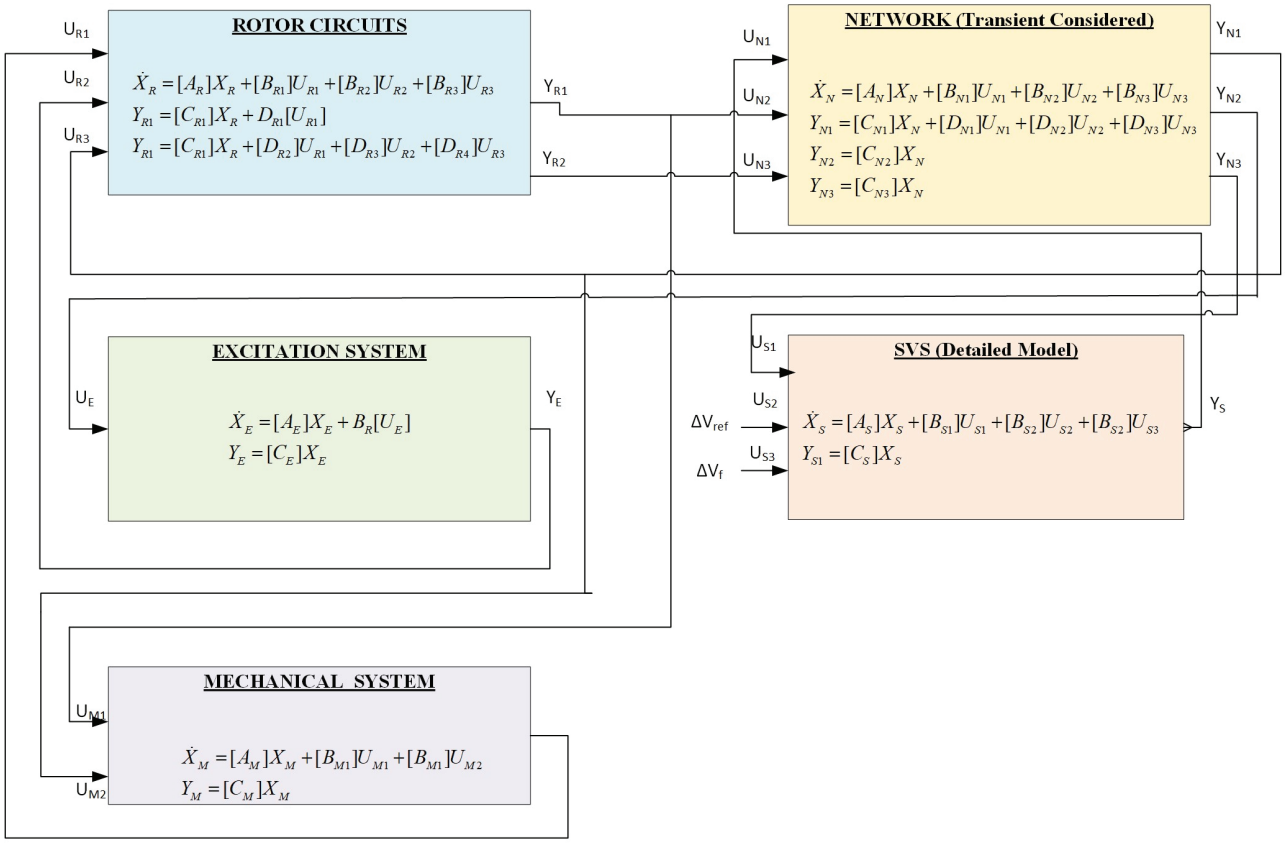

Figure 6. System model.

Let (Q) be a symmetrical matrix, (R) (or (K_I)) also a symmetrical matrix, and (K) the feedback matrix. By applying the reduced order Riccati matrix equation:

$$A^T P + PA - PBR^{-1}B^T P + Q = 0 \tag{55}$$

The acceptable solution for (K) is the one that ensures the system remains stable

$$X' = AX' + B(-KX') = (A - BK)X' \tag{56}$$

To ensure stability, all the eigenvalues of the matrix (A - BK) must have negative real parts. The control law is typically designed to minimize this cost, ensuring system stability and optimal performance. However, solving this optimization problem for the control gain matrix K is challenging, especially for nonlinear or high-dimensional systems. This is where metaheuristic optimization methods like CS-GWO come into play.

Hybrid CSA-GWO Technique

The Purposed (algorithm combines the cuckoo search (CS)[19] for its excellent global search capabilities with the grey wolf optimization (GWO), known for its efficient local search. This hybridization ensures better convergence speed and solution quality compared to the individual algorithms

Grey Wolf Optimization (GWO)

Grey Wolf Optimization mimics the social hierarchy and hunting mechanism of grey wolves. The GWO algorithm categorizes wolves into four types: alpha (leader i.e m), beta (n), delta(o), and omega (follower wolves). The wolves' positions are updated based on the best solutions found (m, n and o wolves), guiding the search toward optimal solutions.

Mathematical Model

An outline of the Grey Wolf Optimizer (GWO) algorithm follows the presentation of the mathematical models for tracking, surrounding, attacking, and social hierarchy in this section.

Social Hierarchy

In the mathematical model of the social structure of wolves in the GWO, the strongest and most resilient solution is represented as alpha (m). Conversely, the solutions ranked second and third are denoted as beta (n) and delta (o) correspondingly. Other candidate solutions are denoted as omega (x). The optimization process is guided by m, n, and o, with the remaining wolves following their lead.

Encircling Prey

Grey wolves exhibit encircling behavior during hunting. The mathematical representation of this behavior is described by the following equations:

$$\vec{D}_1 = \left|\vec{C}_1.\vec{X}_Q(k) - \vec{X}(k)\right| \quad (57)$$

$$\vec{X}(k+1) = \vec{X}_Q(k) - \vec{A}_1.\vec{D}_1 \quad (58)$$

In this context, the variable k represents the current iteration, whereas $\vec{A}_1$ and $\vec{C}_1$ are 'coefficient vectors'. $\vec{X}_Q$ refers to the 'position vectors of the prey', while $\vec{X}$ represents the 'position vector of a grey wolf'. The vectors $\vec{A}_1$ and $\vec{C}_1$ are calculated using specific formulas involving random vectors.

$$\vec{A}_1 = 2\vec{a}.\vec{r}_1 - \vec{a} \quad (59)$$

$$\vec{C}_1 = 2.\vec{r}_2 \quad (60)$$

Hunting

Grey wolves, guided by alpha, exhibit hunting behavior. To simulate this behavior mathematically, the positions of the m (alpha), n (beta), and o (delta) wolves are considered more informed about the potential prey location. The positions of other wolves, including the omegas, are then updated based on these informed positions:

$$\vec{D}_m = \left|\vec{C}_a.\vec{X}_m - \vec{X}\right| \quad (61)$$

$$\vec{D}_n = \left|\vec{C}_b.\vec{X}_n - \vec{X}\right| \quad (62)$$

$$\vec{D}_o = \left|\vec{C}_c.\vec{X}_o - \vec{X}\right| \quad (63)$$

$$X_a = \vec{X}_m - \vec{A}_a.(\vec{D}_m) \quad (64)$$

$$\vec{X}_b = \vec{X}_n - \vec{A}_b.(\vec{D}_n) \quad (65)$$

$$\vec{X}_c = \vec{X}_o - \vec{A}_c.(\vec{D}_o) \quad (66)$$

$$\vec{X}(k+1) = \frac{\vec{X}_m + \vec{X}_n + \vec{X}_o}{3} \quad (67)$$

This approach ensures that the search agents, except for the top three, update their positions according to the more knowledgeable alpha, beta, and delta wolves. These mathematical formulations and algorithms capture the essence of the GWO, where social hierarchy, encircling prey, and hunting behaviors are translated into mathematical models for optimization purposes.

CUCKOO SEARCH ALGORITHM (CSA)

The natural world is home to more than a thousand bird species, many of which share characteristics and habits. As an example, all bird mothers build nests in safe areas and deposit eggs in a variety of forms to ward off predators. Mother birds, for instance, construct nests in safe areas to shield their young from predators and lay eggs in a variety of designs. The cuckoo is a well-known brood parasite, renowned for its deceptive strategy. A female cuckoo will remove one of the host's eggs and replace it with her own, mimicking the appearance of the host's eggs to avoid detection. This ensures that the cuckoo egg hatches first, and the cuckoo chick often evicts the host's eggs from the nest, securing all resources for itself. This action served as inspiration for Yang and Deb's Cuckoo Search Algorithm (CSA) [20]. It is a productive optimization technique that strikes a balance between regional and global exploration. CSA is based on three main rules:

1. Each cuckoo deposits a single egg in a nest chosen at random.
2. Nests of superior quality, containing high-grade eggs, are passed down to future generations.
3. There is a set number of host nests and the probability that a host bird finds an alien egg is Ba ∈ (0, 1). When a host bird's eggs are found, it can either drop them or leave the nest to start a new one. The number of available host nests stays the same, and the chance that a host bird will lay an egg laid by an alien is Ba, where Ba can take on values between 0 and 1. The host bird will either leave the nest or drop the egg once it's found. Then it will start building a new nest. The Pseudo code of the CS-GWO algorithm is shown in Figure 7.

The algorithm can be succinctly summarized in the subsequent steps:

1. Objective function f(Z), where Z = (z1, z2……,zd)T
2. Establish the starting population of n host nests
3. While loop, until a halt criterion is satisfied(e.g., maximum iterations or generations):
   - Obtain a cuckoo through random movements following Lévy flights.
   - Assess the suitability of its fitness in terms of K_x and K_y.
   - Select a random nest y from the set n.
   - If $K_x > K_y$, substitute y with the revised solution.
   - Discard a portion B_a of the least favorable nests and construct new ones.
   - Retain the optimal options and arrange them in order of preference.

The Lévy flight mechanism is key to CSA, as it enables a balance between exploration and exploitation:

$$z_{t+1}^i = z_t^i + \alpha \oplus Lévy(\lambda) \quad (68)$$

where α>0 is the step size, and ⊕ denotes entry wise multiplication. Lévy flights are characterized by:

$$Lév \sim u = t^{-\lambda}, \quad 1 < \lambda \leq 3 \quad (69)$$

```
Initialize the grey wolf population Xa(a=1,2,3,...n)
Initialize a, A, C,and pa
Calculate the fitness of each search agent (wolf)
Xm-the best search agent
Xn=the second best search agent
Xo=the third best search agent
While (t<Max number of iterations)
    for each search agent
       Update the position of current search agent by equation (40)
    end
Update a, A, and C
Calculate the fitness of all search agents
Update Xm , Xn and Xo
Update the wolf's position by equation (66).
   if random number> pa then
random change the wolf's position.
Compute and update the fitness function
t=t+1
  end while
return best solution Xm
```

Figure 7. Pseudo code of CS-GWO algorithm.

Table 2. Comparative Analysis of CSA, GWO, and Hybrid CSA-GWO for Optimization Efficiency

Feature	Cuckoo Search Algorithm (CSA)	Grey Wolf Optimizer (GWO)	Hybrid CSA-GWO
Inspiration	Brood parasitism of cuckoo birds	Leadership hierarchy of grey wolves	Combination of CSA and GWO principles
Exploration	Strong due to Lévy flight	Moderate due to leader-based search	Enhanced due to hybridization
Exploitation	Moderate	Strong due to adaptive leadership	Balanced through adaptive switching
Convergence Speed	Can be slow in large search spaces	Faster due to hierarchical structure	Improved due to hybrid approach
Optimization Accuracy	Good for global search	Good for local refinement	High accuracy with adaptive tuning
Application in SSR Mitigation	Effective but may require tuning	Effective in dynamic conditions	Superior due to adaptive and efficient tuning

The flow chart for CSA-GWO is shown in Figure 8. This process ensures that some solutions are explored globally, while others exploit the local area around the current best solution.

The performance comparison of CSA, GWO, and the hybrid CSA-GWO algorithm is summarized in Table 2, highlighting their optimization efficiency and key characteristics. The Hybrid Cuckoo Search and Grey Wolf Optimization (CS-GWO) is a powerful optimization technique for solving complex control system problems, such as designing optimal controllers. By combining the exploration capabilities of CS with the exploitation strengths of GWO, this hybrid algorithm is well-suited for finding optimal control gain matrices that minimize the system›s performance cost. The hybrid CS-GWO approach demonstrates fast convergence, robustness, and high solution quality, making it a valuable tool in modern control system design.

RESULTS AND DISCUSSION

Case A : System without Natural Damping

For a system delivering (Pg = 800) MW, the eigenvalues were calculated under various scenarios: with and without

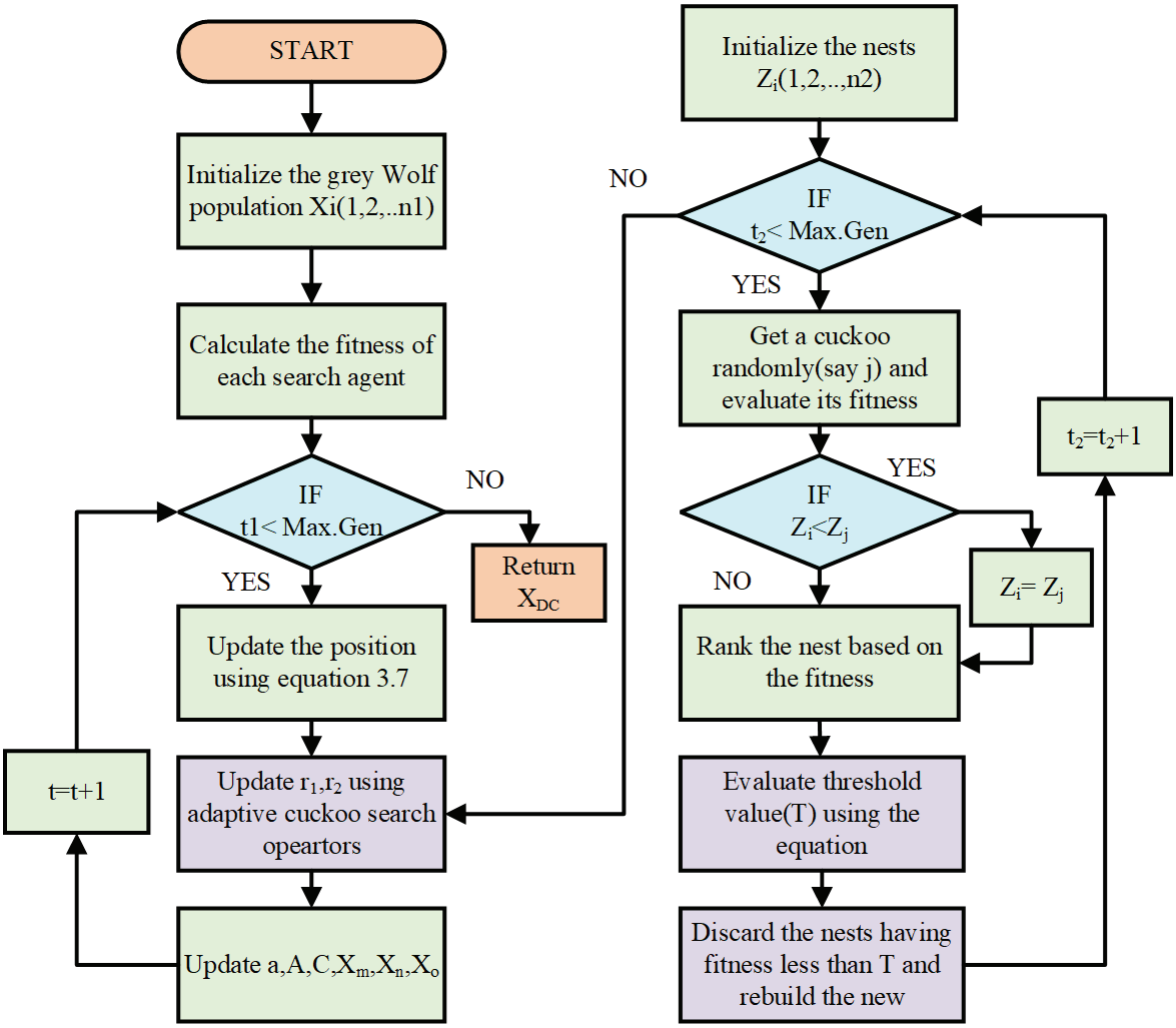

Figure 8. Flowchart of cuckoo-grey wolf proposed algorithm.

the application of optimal control, with zero natural damping, all within a series-compensated network and 10% change in electric torque and 10% change in reference voltage. As shown in Table 3 compares the system eigenvalues under different control strategies—SVS only, optimal controller, BFOA-based controller, and the proposed hybrid CSA-GWO controller at 50% compensation without natural damping. The results show that the hybrid CSA-GWO controller achieves the most significant leftward eigenvalue shift, enhancing system damping and stability. Key improvements include reduced oscillations in generator modes, better network stability, and superior performance of SVC and AVR, leading to more effective mitigation of SSR and improved turbine-generator dynamic performance.

Figure 9 depicts the mechanical rotor angle (MECH-DELTA (RAD)), showcasing the rotor›s dynamic response. Figure 10 presents the HP-IP Torque (P.U), highlighting the torque variations in the high-pressure and intermediate-pressure turbine stages. Figure 11 shows the SVC Bus Voltage, demonstrating the voltage regulation at the bus controlled by the Static Var Compensator (SVC). Lastly, Figure 12 illustrates the SVC Susceptance (P.U), reflecting the changes in the SVC›s reactive power compensation to maintain voltage stability.

The transient response characteristics of the system under investigation are evaluated based on Table 4, which presents the time-domain analysis (T.D.A) for the rotor angle curve without natural damping. A comparative assessment is made between the SVS-only system and the optimal controller, BFO-optimized controller, and hybrid CSA-GWO technique to determine their effectiveness in improving system stability.

For rise time, all three control strategies result in an increase compared to SVS-only (0.59301 s). The optimal controller alone shows an increase of 41.8%, while the BFO-optimized controller and hybrid CSA-GWO method exhibit increases of 40.3% and 37.4%, respectively. Despite this, the controlled systems demonstrate better performance in other critical stability measures.

Table 3. System eigenvalue for case A at 50% compensation without natural damping

Mode	With SVS Only	With optimal controller	With optimal controller & BFO [18]	With optimal controller &Hybrid CS-GWO (Proposed study)
Mode 5	7.0129e-05±298.18i	-0.42252±298.18i	-0.42258± 298.18i	-0.5±298.18i
Mode 4	-0.11323±203.01i	-6.5595±202.91i	-6.5668±202.91i	-6.812±202.91i
Mode 3	-0.089727±160.77i	-7.9616±160.76i	-7.9655±160.76i	-8.0±160.76i
Mode 2	-0.018756±127.06i	-5.8125±128.31i	-5.8132±128.31i	-5.92±128.31i
Mode 1	0.0306±99.6767i	-7.4304±98.8561i	-7.4306±98.8562i	-7.491±98.8562i
Mode 0	-2.0265±13.6598i	-2.9213±12.6086i	-2.9214±12.6052i	–3.13±12.6052i
Network	-3.2878±3497.1i	-3.2882±3497.1i	-3.3192±3497.1i	-4.1950±000.0i
	-3.2880±2868.8i	-3.2888±2868.8i	-3.3484+2868.8i	-3.459±2868.8i
	-13.911±2528.9i	-13.913±2528.9i	-14.029±2528.9i	-14.57±2528.9i
	-15.861±1900.7i	-15.867±1900.7i	-16.133±1900.7i	-17.012±1900.7i
	-12.490±1120.8i	-18.919±1121.4i	-50.065± 1125.3i	-50.98±1125.3i
	-18.929±493.31i	-58.218±498.67i	-66.235±493.65i	-67.01±493.65i
	-11.854±328.38i	-371.39±366.05i	-1585.1± 453.73i	-1589.42±453.73i
	-3.3187±315.07i	-11.839+328.30i	-11.839±328.30i	-12.49±328.30i
	-11.698±299.62i	-11.815 ±299.63i	-11.815±299.64i	-12.45±299.64i
Generator system	-32.3668	-51.4780	-51.4780	-52.623
	-24.8779	-30.4181	-30.4182	-31.578
	-1.9448	-5.7939	+5.7939	±5.7i
SVC	-545.08	-625.19	-804.95	-810.45
	± 72.704i	-447.95	-417.13	-419.74
	-55.4864	-165.53	-169.20	-170.68
	±92.8421i	±351.39i	±333.78i	±333.0i
	-2.9118	-127.40	-127.71	-130.0
	±310.64i	-1.7614	-1.7816	-1.865
AVR	-26. 1307	-0. 14624	-0.14624	-0.14624
	±24.1266i	±314.16i	±314.16i	±314.16i
	-0.6407	-0.9066	-0.9066	-0.9066
	±1.2882i	±1.2882i	±1.2747i	±1.298i

Table 4. T.D.A for the rotor angle curve without natural damping

MECH-DELTA (rad.)	With SVS only	With optimal controller	With optimal controller and BFO	With optimal controller and Hybrid CS-GWO
Rise time	0.59301 s	0.84108 s	0.83252 s	0.81430 s
Settling time	24.99 s	4.5629 s	3.3641 s	2.3732 s
Over-shoot	32.563	18.83	17.968	17.461
Under-shoot	0	0	0	0
Peak time	1.62 s	1.88 s	1.86 s	1.73 s

A significant improvement is observed in settling time across all controllers compared to SVS-only (24.99 s). The hybrid CSA-GWO technique achieves the most improvement with a change of 90.5%, followed by the BFO-optimized controller at 86.5% and the optimal controller alone at 81.7%. This substantial enhancement highlights the controllers› effectiveness in enhancing system damping and stability.

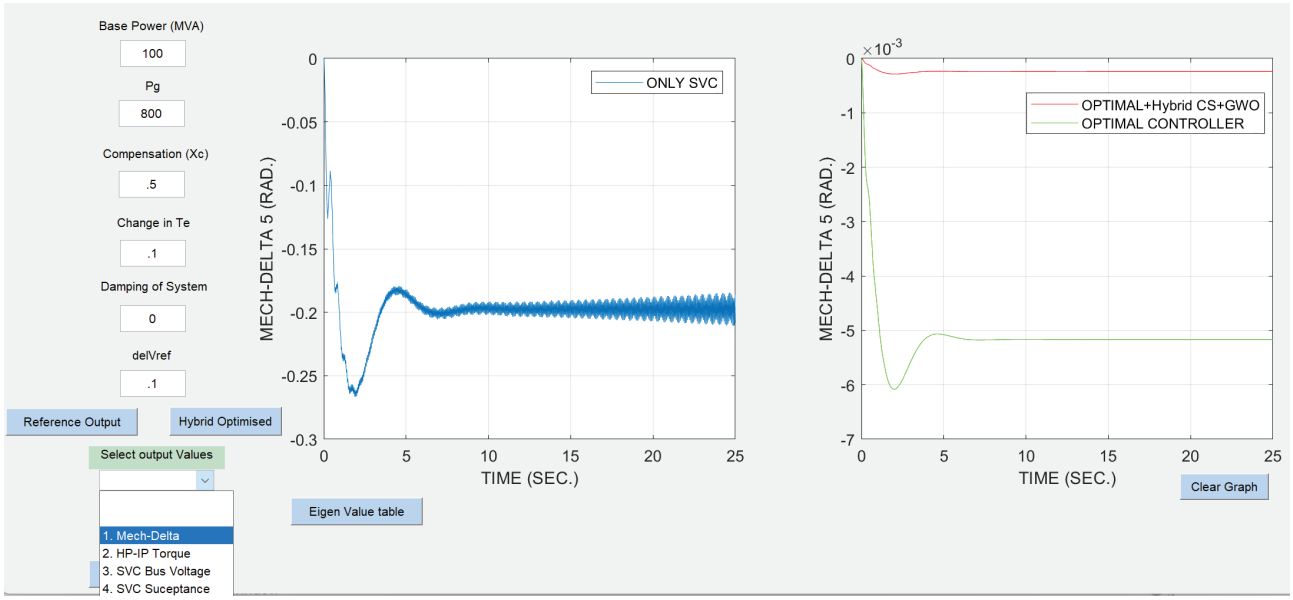

Figure 9. Mech-delta (rad) of case A.

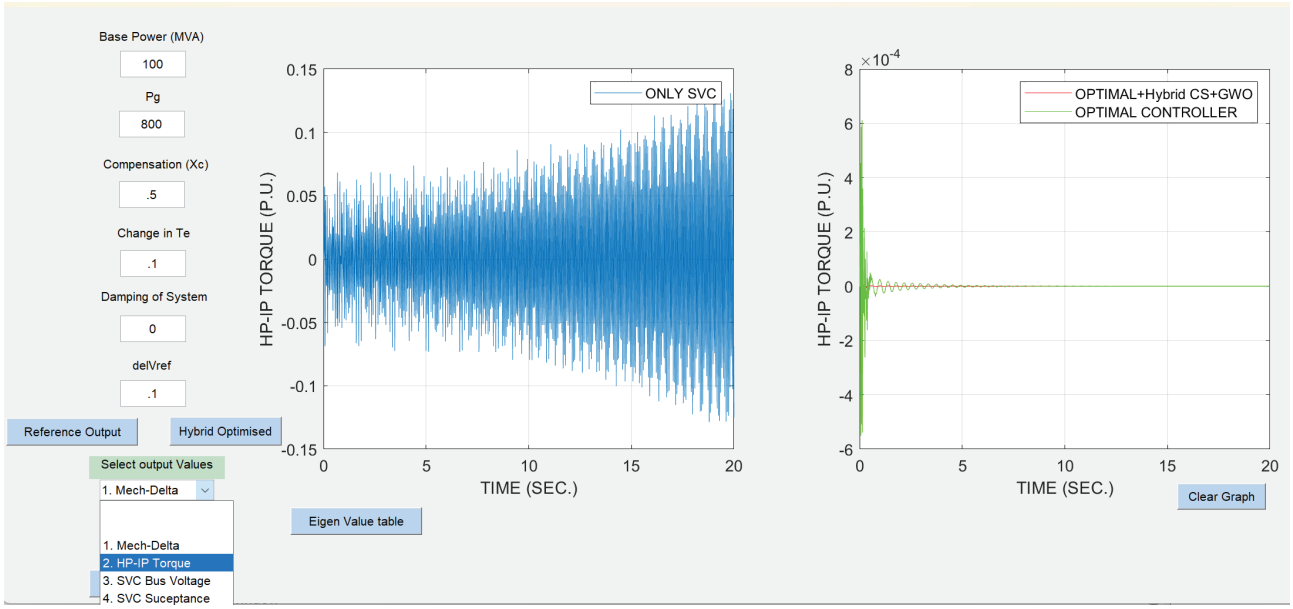

Figure 10. HP-IP torque (P.U) of case A.

In terms of overshoot, the hybrid CSA-GWO method exhibits the most improvement (46.4%) over the SVS-only case (32.563), followed by BFO-optimized (44.8%) and the optimal controller alone (42.2%). A lower overshoot indicates a more controlled system response with minimal excessive fluctuations.

For peak time, the hybrid CSA-GWO method achieves the smallest increase at 6.8%, making it the best performer in this aspect. In contrast, the BFO-optimized controller shows an increase of 14.8%, while the optimal controller alone exhibits a 16.0% increase compared to SVS-only (1.62 s). The controlled systems maintain zero undershoot across all cases, ensuring no negative oscillations or system instability.

The hybrid CSA-GWO technique outperforms all other methods, achieving the best improvement in settling time and overshoot with minimal peak time variation. While the BFO-optimized and optimal controllers show strong performance, hybrid CSA-GWO remains the most effective for system stability and transient response

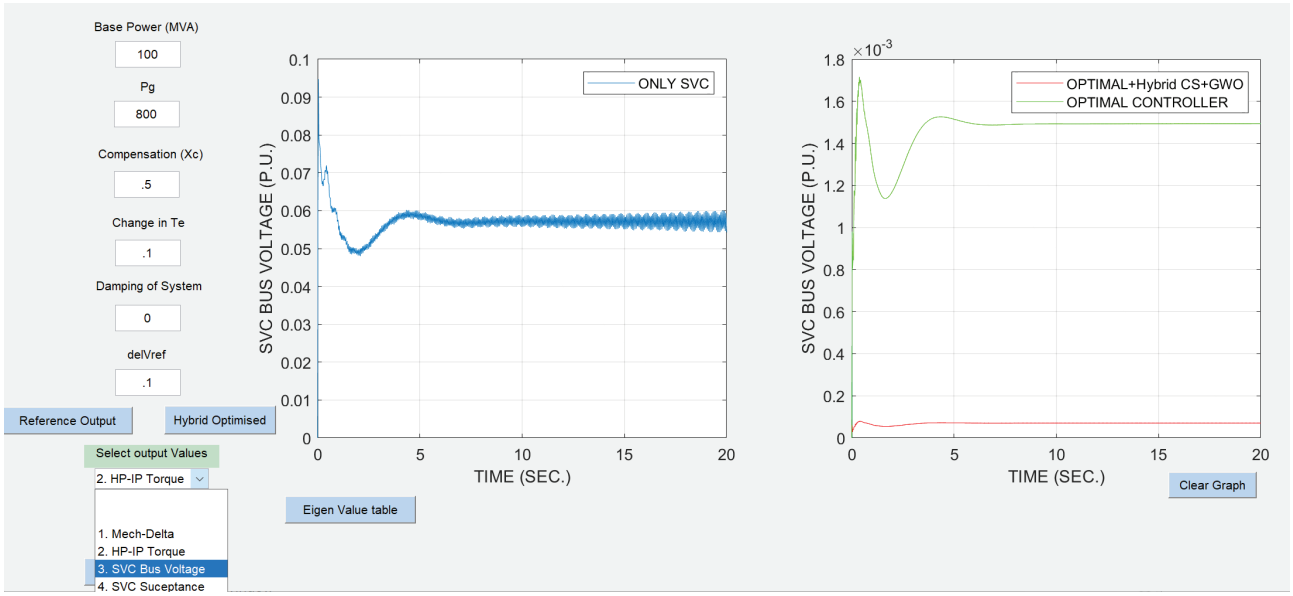

Figure 11. SVC bus voltage of case A.

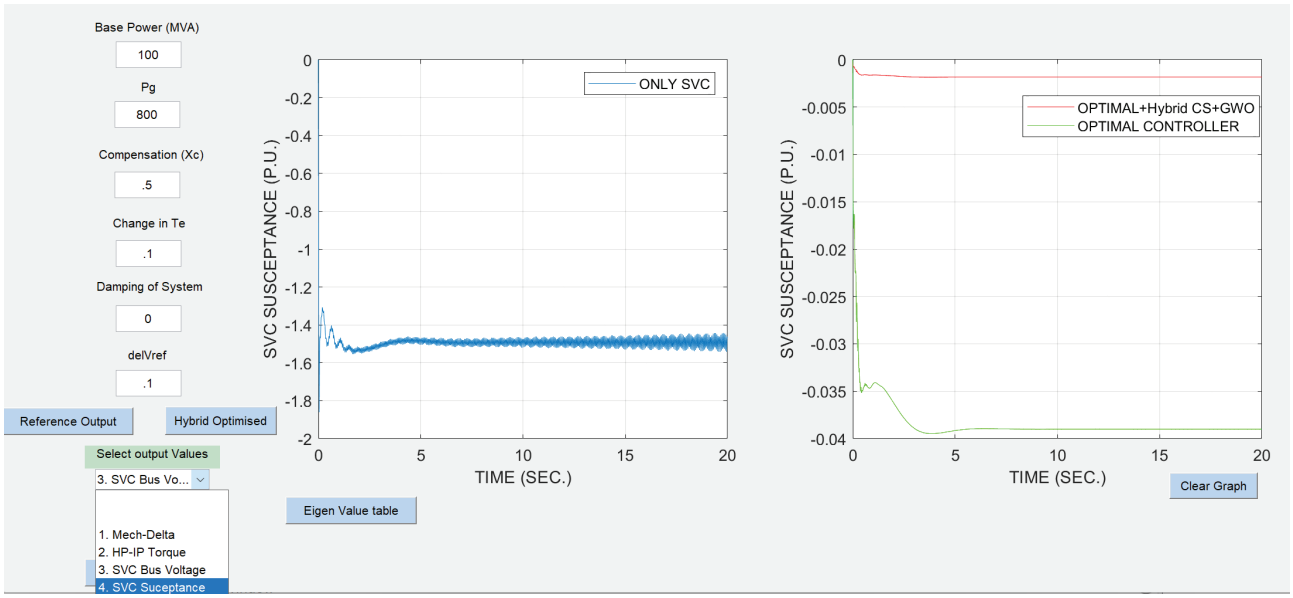

Figure 12. SVC susceptance (P.U) of case A.

Case B: System with Natural Damping

The system›s response is illustrated after a 10% change in electric torque and a 10% change in reference voltage, and analyzed under 50% compensation while considering inherent damping effects (D = 0.0322). Table 5 presents eigenvalues, assessing stability, while Figure 13 and Figure 14 illustrate rotor angle and HP-IP torque dynamics, respectively. Voltage stability at the SVC bus is depicted in Figures 15 and 16, offering insights into system reliability..

Table 5 compares eigenvalues for different control strategies SVS only, optimal controller, BFOA-based controller, and the proposed hybrid CSA-GWO controller. The results indicate that the hybrid CSA-GWO controller shifts eigenvalues further left in the complex plane, significantly improving system damping. This leads to reduced oscillations in critical modes, enhanced network stability, and better performance of the SVC and AVR, ensuring more effective mitigation of SSR and improved dynamic performance of the turbine-generator system.

Table 5. System eigenvalue for case B at 50% compensation with natural damping (D=0.0322)

Mode	With SVS Only	With optimal controller	With optimal controller & BFO [18]	With optimal controller &Hybrid CS-GWO (Proposed study)
Mode 5	7.0129e-05±298.18i	-0.42252±298.18i	-4.4484±298.14i	-4.4484± 294.14i
Mode 4	-0.11323±203.01i	-6.5595 ± 202.91i	-7.1784±202.88i	-7.1789±202.88i
Mode 3	-0.089727±160.77i	-7.9616 ±160.76i	-8.1888±160.65i	-8.1892 ± 160.65i
Mode 2	-0.018756±127.06i	-5.8125 ±128.31i	-11.868±127.73i	-11.868±124.73i
Mode 1	0.0306±99.6767i	-7.4304±98.8561i	-7.5498±99.0542i	-7.5499±99.0542i
Mode 0	-2.0265±13.6598i	-2.9213±12.6086i	-3.6804±12.5053i	-3.6806±12.5049i
Network	-3.2878±3497.1i	-3.2882±3497.1i	-3.3143±3497.1i	-3.3133 ±3497.1i
	-3.2880±2868.8i	-3.2888±2868.8i	-3.3402±2868.8i	-3.3377 ±2868.8i
	-13.911±2528.9i	-13.913±2528.9i	-14.015±2528.9i	-14.981 ±2528.9i
	-15.861± 1900.7i	-15.867±1900.7i	-16.112±1900.7i	-17.012 ±1900.7i
	-12.490±1120.8i	-18.919±1121.4i	-49.502 ± 1125.3i	-72.502 ± 1130.3i
	-18.929± 493.31i	-58.218±498.67i	-66.222±493.67i	-68.322±493.67i
	-11.854± 328.38i	-371.39±366.05i	-1450.8± 563.85i	-1758.8 ± 726.85i
	-3.3187±315.07i	-11.839+328.30i	-11.839±328.30i	-11.839 ±321.30i
	-11.698±299.62i	-11.815±299.63i	-11.815±299.63i	-11.815±299.63i
Generator system	-32.3668	-51.4780	-51.1758	-51.1758
	-24.8779	-30.4181	-30.4163	-30.4163
	-1.9448	-5.7939	-5.7792	-5.7792
SVC	-545.08	-625.19	-800.79	-823.74
	± 72.704i	-447.95	-417.20	-402.60
	-55.4864	-165.53	-169.22	-169.22
	±92.8421i	±351.39i	±333.82i	±333.82i
	-2.9118	-127.40	-127.84	-127.92
	±310.64i	-1.7614	-1.7742	-1.7934
AVR	-26. 1307	-0. 14624	-0.14624	-0.14624
	±24.1266i	±314.16i	±314.16i	±314.16i
	-0.6407	-0.9066	-0.8997	-0.8997
	±1.2882i	±1.2882i	±1.2762i	±1.2631i

Table 6 provides a time-domain analysis (T.D.A) of the rotor angle curve, evaluating key performance metrics. For rise time, all controllers exhibit an increase compared to the SVS-only system (0.61326 s). The optimal controller shows a 38.4% increase, while the BFO-optimized controller and hybrid CSA-GWO method result in increases of 37.2% and 46.4%, respectively.

Examining settling time, the hybrid CSA-GWO method achieves the highest improvement with a 60.1% change, followed by the BFO-optimized controller at 36.6% and the optimal controller alone at 12.7%, compared to the SVS-only system (5.3236 s).

For overshoot, the hybrid CSA-GWO technique exhibits the most improvement with a 47.1% change, while the BFO-optimized controller and optimal controller achieve changes of 44.6% and 41.9%, respectively, over the SVS-only case (32.715).

Considering peak time, the hybrid CSA-GWO method results in the smallest increase at 4.7%, making it the most effective in this aspect. In comparison, the BFO-optimized controller and optimal controller show increases of 11.9% and 14.3%, respectively, over the SVS-only system (1.68 s).

The hybrid CSA-GWO technique emerges as the most effective control strategy, offering the highest improvement in key stability parameters. It excels in settling time and overshoot while ensuring minimal deviation in peak time, making it the best choice for enhancing overall system performance.

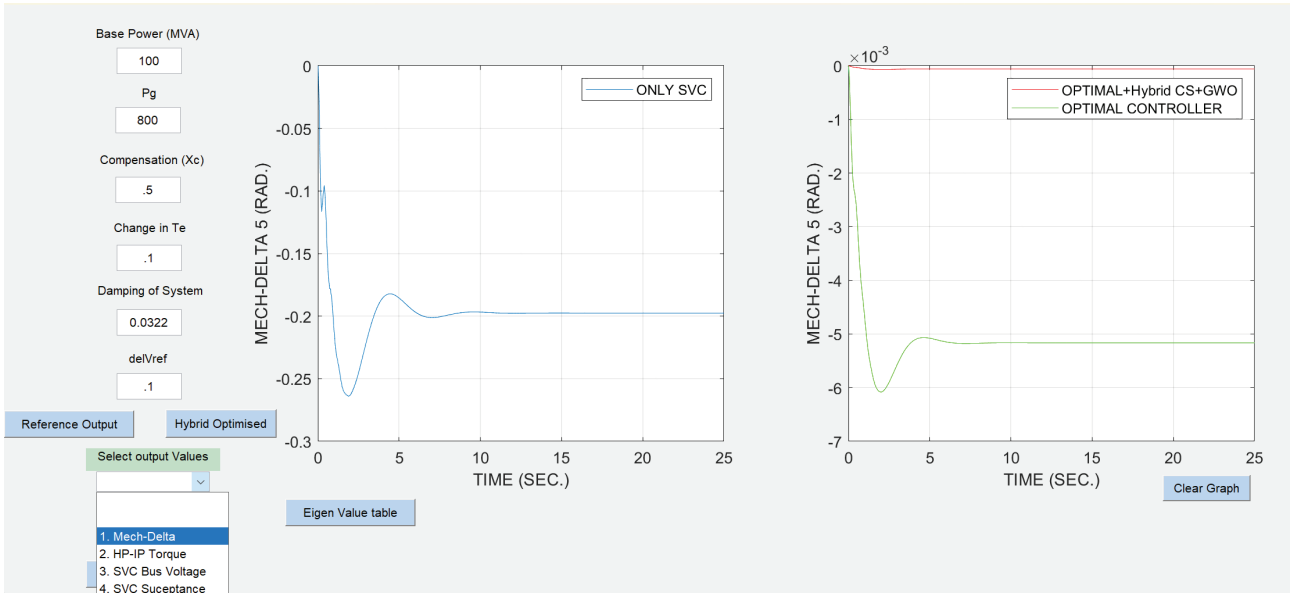

Figure 13. Mech-delta (RAD) of case B.

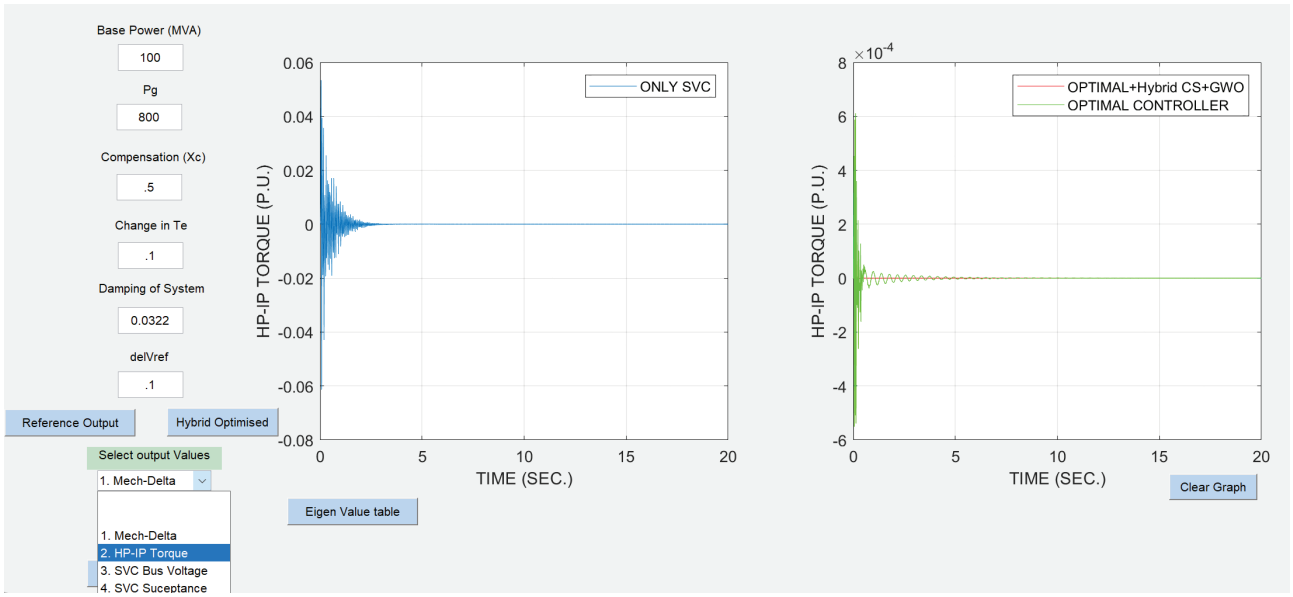

Figure 14. HP-IP torque (P.U) of case B.

Table 6. T.D.A for the rotor angle curve with natural damping

MECH-DELTA (rad.)	With SVS only	With optimal controller	With optimal controller and BFO	With optimal controller and Hybrid CS-GWO
Rise time	0.61326 s	0.84882 s	0.84142 s	0.89732 s
Settling time	5.3236s	4.6479 s	3.3735 s	2.1246 s
Over-shoot	32.715	18.993	18.11	17.325
Under-shoot	0	0	0	0
Peak time	1.68 s	1.92 s	1.88 s	1.76 s

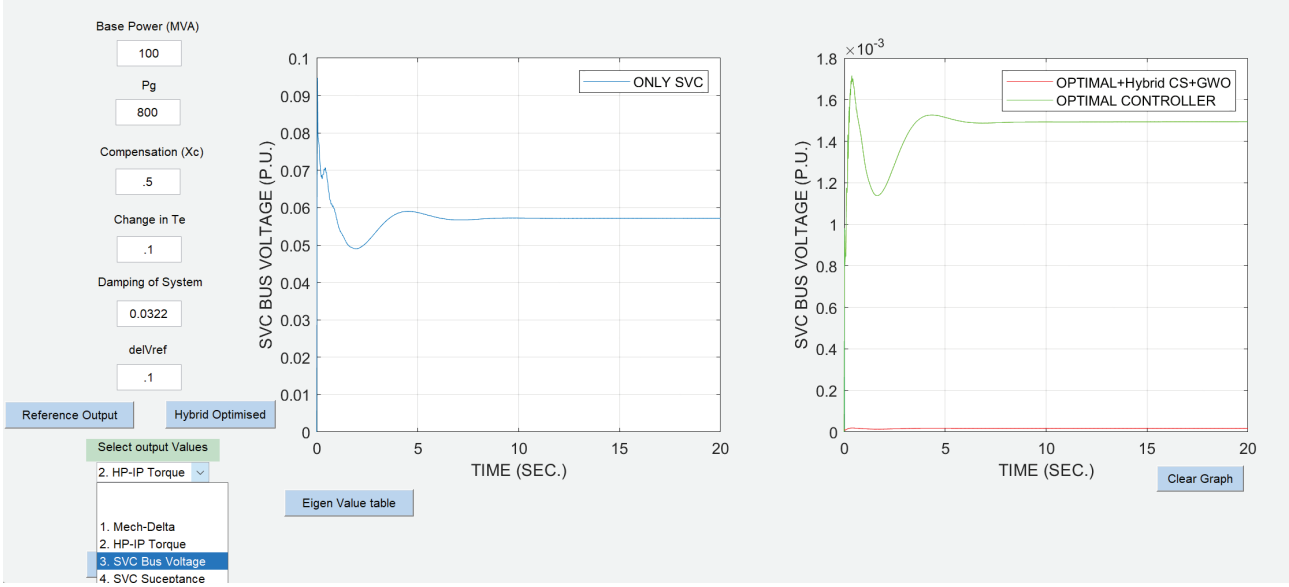

Figure 15. SVC bus voltage of case B.

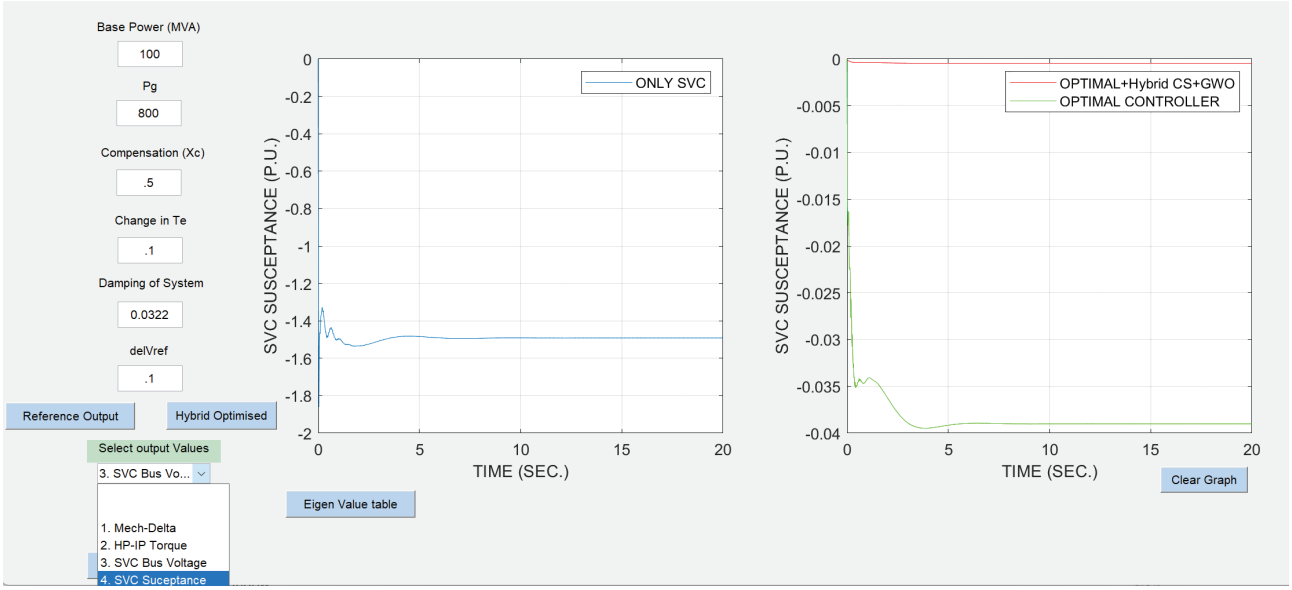

Figure 16. SVC bus voltage of case B.

CONCLUSION

In this paper, an investigation is conducted to examine the effectiveness of a Hybrid Cuckoo Search Algorithm-Grey Wolf Optimization (CSA-GWO)-based control strategy for Static Var Compensator (SVC) in mitigating sub-synchronous resonance (SSR) and enhancing the stability of turbine-generator systems in series-compensated networks. Using the IEEE First Benchmark Model, the proposed Hybrid CSA-GWO algorithm proves to be more effective than BFO, achieving faster damping of harmful oscillations, superior transient stability, and enhanced steady-state performance. Fluctuations in electric torque and reference voltage intensify SSR, increasing control complexity and system instability. The study evaluates both natural damping and zero damping cases, with zero damping included to analyze the system under more severe conditions. Eigenvalue analysis and time-domain simulations confirm that the Hybrid CSA-GWO method consistently outperforms BFO, proving to be the most effective solution for mitigating SSR, improving transient response, and ensuring grid resilience.

Future Scope

Building on this research, the following key areas offer promising directions for further enhancement of SSR mitigation and power system stability.

1. Real-Time Implementation: Validate the CSA-GWO-based controller in real-world power systems using hardware-in-the-loop (HIL) simulations and prototype testing.
2. Adaptive Control Strategies: Develop adaptive and self-tuning controllers that dynamically adjust based on real-time system conditions for improved SSR mitigation.
3. Multi-Machine System Analysis: Extend the study to multi-machine power systems to evaluate effectiveness in complex network scenarios.
4. Integration with Renewable Energy Sources: Investigate the impact of renewable energy sources like wind and solar on SSR mitigation and overall system stability.
5. Machine Learning Applications: Implement AI/ML-based predictive control for real-time SSR detection and mitigation, enhancing system resilience.

NOMENCLATURE

Ψ_f	Flux associated with coil 'f'
Ψ_h	Flux associated with coil 'h'
Ψ_g	Flux associated with coil g
Ψ_k	Flux associated with coil 'k'
i_d and i_q	are the d-axis and q-axis components of the machine terminal currents
M_i	Inertia of ith mass
Di	Damping of ith mass
K_{ij}	Spring constants of the shaft elements between mass i and j
Di	Damping of shaft segments between mass i and j
δ_{M2}	Angular position of HP turbine
δ_{M3}	Angular position of IP turbine
δ_{M4}	Angular position of LPA turbine
δ_{M5}	Angular position of LPB turbine
δ_{M6}	Angular position of GEN
δ_{M7}	Angular position of exciter
ω_1	Angular velocity of HP turbine
ω_2	Angular velocity of IP turbine
ω_3	Angular velocity of LPA turbine
ω_4	Angular velocity of LPB turbine
ω_5	Angular velocity of LPB turbine
S_E	Saturation function
V_F	Excitation voltage of gen.
V_S	Stabilizing feedback signal voltage
V_f	Excitation system regulator's output voltage
L_{T1}	Inductance of sending end transformer
L_{T2}	Inductance of receiving end transformer
Ra	Armature resistance of the synchronous generator
I	Dependent current source equivalent of generator
V_g	Vs generator terminal voltage
lg	Generator terminal current
i_{gd}	Gen. terminal current associated with direct axis
i_{gq}	Gen. terminal current as sociated with quadratur axis
Y_{shr}	Shunt admittance at receiving end
Y_{shs}	Shunt admittance at sending end
C_{ses}	Series capacitance at sending end
C_{ser}	Series capacitance at receiving end
V_1	Infinite bus voltage
i_1	Incoming current of infinite bus
V_i	Voltage at bus represented by its subscripts (i= 1 to 5)
V_6	Voltage at sending end series capacitor
V_{5RCD}	Voltage at receiving end series capacitor
i_I	Current in the different sections of network
i_3	TCR current
i_x	Net current injected by SVC
ix'	Current through shunt capacitance at SVC bus
C_n	Fixed capacitance of SVC
Z_1	Regulator block input
Z_2	Measurement unit output
Z_3	Regulator block output of SVS
B	Susceptance offered by SVS
K_{iD}	Constant of SVC system associated with i3D
K_{iQ}	Constant of SVC system associated with i3Q
K_{vD}	Constant of SVC system associated with V3D
K_{vQ}	Constant of SVC system associated with V3D
X_e	Capacitive-reactance of compensating capacitor
X_{se1}	Series compensation reactance at sending end
X_{se2}	Series compensation reactance at sending end
δ,R,L	Power angle ,resistance, inductance for Line
P,Q,V,θ	Real power, reactive power, voltage,bus voltage angle at different buses.
T_E	electrical torque
K_P,K_I	Proportional, integral gains of SVS voltage controller
G	Gain of SVS
K_D	Slope of control characteristics
T_S, T_D,T_M	FIring delay,thyristor delay, measurement time constant
V_F	Auxiliary control signals
I_D,I_Q	D and Q axis components of la currents of the 'generator
x_1	Stator leakage reactance
x_d, x_d', x_d''	Direct axis synchronous, transients and sub transients reactance, respectively
x_q, x_q', x_q''	Quadrature axis synchronous transients and sub transients reactance, respectively
T_{do}',T_{do}''	Direct axis transients and sub transients open circuit time constants, respectively.
T_{qo}',T_{qo}''	Quadrature axis transients and sub transients open circuit time constants, respectively.
I_g	Generator current
HP	High pressure turbine
IP	Intermediate pressure turbine
LPA	Low pressure turbine A

LPB	Low pressure turbine B
GEN	Generator
EXC	Exciter
P_E	Electrical power output from generator
P_M	Mechanical power input to the generator

Subscripts:

R, M, E, N	rotor circuit, mechanical, excitation, network
f, h, g, k	field and amortisseur circuits
D. Q, 0	D-Q-0 axis variable (stator frame of reference)
d, q, 0 : d-q-0	axis variable (rotor frame of reference)

AUTHORSHIP CONTRIBUTIONS

Authors equally contributed to this work.

DATA AVAILABILITY STATEMENT

The authors confirm that the data that supports the findings of this study are available within the article. Raw data that support the finding of this study are available from the corresponding author, upon reasonable request.

CONFLICT OF INTEREST

The author declared no potential conflicts of interest with respect to the research, authorship, and/or publication of this article.

ETHICS

There are no ethical issues with the publication of this manuscript.

STATEMENT ON THE USE OF ARTIFICIAL INTELLIGENCE

Artificial intelligence was not used in the preparation of the article.

REFERENCES

[1] Farmer RG, Schwalb AL, Katz E. Navajo project report on subsynchronous resonance analysis and solutions. IEEE Xplore 1977;96:1226–1232. [CrossRef]

[2] Anderson PM, Agrawal BL, Ness JEV. Sub-Synchronous Resonance in Power System. 1st ed. New York: IEEE Press; 1990.

[3] Farmer RG, Schwalb AL, Katz E. Navajo project report on subsynchronous resonance analysis and solutions. IEEE Xplore 1977;96:1226–1232. [CrossRef]

[4] Walker DN, Bowler CEJ, Jackson RL, Hodges DA.Results of subsynchronous resonance test at Mohave. IEEE Xplore 1975;94:1878–1889. [CrossRef]

[5] Padiyar K. Facts Controllers in Power Transmission and Distribution. New Delhi, India:New Age International Publishers 2007.

[6] Kumar N, Dave MP. Application of an auxiliary controlled static var system for damping subsynchronous resonance in power systems. Electr Power Syst Res 1996;37:189–201. [CrossRef]

[7] Padiyar KR, Prabhu N. Design and performance evaluation of subsynchronous damping controller with STATCOM. IEEE Xplore 2006;21:1398–1405. [CrossRef]

[8] Prada M, David FM, Garcia JLD, Muljadi E, Singh M, Bellmunt OG, et al., Contribution of type-2 wind turbines to sub-synchronous resonance damping. Int J Electr Power Energy Syst 2014;55:714–722. [CrossRef]

[9] Bamba S, Gupta SK. Enhancing power system stability through intelligent STATCOM control strategies in torsional oscillation environments. Sigma J Eng Nat Sci 2024. [CrossRef]

[10] Wadhwa K, Gupta SK. Analysing the Design and Performance of a Controller for AGC in Multi-Source Systems Using Cuckoo Search Optimization. IEEE Xplore 2023;1–5. [CrossRef]

[11] Arockiaraj S, Manikandan BV, Alagammal S, Bhavani R. Sub synchronous resonance analysis of inverter-based wind and solar farms using genetic widow optimization. J Power Electron 2024;24:1516–1526. [CrossRef]

[12] Wang L, Lai JT, Li TY, Tseng CC, Mokhlis H, Chua KH. Suppression of Subsynchronous Resonance in a Hybrid Steam-Turbine Generator/Offshore Wind Farm System Using a Static Synchronous Compensator with a Vanadium Redox Flow Battery. IEEE Xplore 2025;1–8. [CrossRef]

[13] Bamba S, Gupta SK. Sub-Synchronous Resonance Mitigation in Series-Compensated Power Systems Using a GWO-Based Optimal Controller. IEEE Xplore 2023. [CrossRef]

[14] Soeprijanto A, Abdillah M. Subsynchronous Resonance Damping Using SMES Optimized By Quantum Behaved Particle Swarm Optimization. 3rd International Conference on Advances in Computing, Control, and Telecommunication Technologies. Jakarta, Indonesia; 2011.

[15] Shivashanker K, Janaki M. Mitigating Torsional Interactions with MMC Connected to Turbine-Generator Using a Novel Subsynchronous Damping Controller. Int J Intell Eng Syst 2025;18: 1275–1290. [CrossRef]

[16] Thota K, Velpula S, Basetti V. A scientometric analysis on DFIG-based wind energy conversion system research trends. Discov Appl Sci 2024;7:7. [CrossRef]

[17] Gupta SK, Gupta AK, Kumar N. Damping subsynchronous resonance in power systems. Inst Eng Technol 2002;149:679–688. [CrossRef]

[18] Gupta SK. Analysis and mitigation of sub-synchronous resonance in power system with svc and using bfo based optimal controller. Int J Recent Sci Res 2014;1:39–44.

[19] Amin MN, Soliman MA, Hasanien HM, Abdelaziz AY. Hybrid CSA-GWO Algorithm-Based Optimal Control Strategy for Efficient Operation of Variable-Speed Wind Generators. Springer 2021;227–245. [CrossRef]

[20] Abraham A. 2009 World Congress on Nature & Biologically Inspired Computing. IEEE 2009.

APPENDIX A.

SVS DATA (quality factor = 100))			
K_I (integral gain in PI controller)	1200sec	T_S (Thyristor delay time constant)	0.005
T_M (Measuring time constant)	0.0024sec	K_D (current droop)	0.01
K_P (Proportional gain in PI controller)	-1	T_D (thyristor avg. dead time)	0.001667

Network Impedances in Per Unit on the Generator MVA Base (100 MVA}, Voltage =400KV, Freq=50Hz			
R	0.012525	XL	0.1197 P.U for whole line
B	3.552	No of conductors	2
Length of line	600km	Area of conductors	0.4inch2
Reactance of line	0.034 ohm/phase/km	Surge impedance	296ohm
Resistance of line	0.0325 ohm/phase/km	Natural load	540MW

Shaft inertia and spring constant for first bench mark model in per unit on Machine base			
Inertia	Inertia Constant H in Sec	Shaft Section	Spring Constant K in pu T/rad
HP Turbine	0.1033586	HP-IP	25.772
IP Turbine	0.1731106	IP-LPB	46.635
LPA Turbine	0.9553691	LPA-LPB	69.478
LPB Turbine	0.9837909	LPB-Gen	94.605
Generator	0.9663006	Gen-Exc	3.768
Exciter	0.03880697		